LBL-19098 Rev.

Presented at the Polymer Processing Society Meeting, Akron, OH, March 28, 1985

PROFILE DEVELOPMENT IN DRAWN HOLLOW TUBES

B.D. Freeman, M.M. Denn, R. Keunings, G.E. Molau and J. Ramos

January 1985

Lawrence Berkeley Laboratory
University of California
Berkeley, California 94720

Prepared for the U.S. Department of Energy
under Contract DE-AC03-76SF00098

Center for Advanced Materials

DISCLAIMER

PROFILE DEVELOPMENT IN DRAWN HOLLOW TUBES

B.D. Freeman, M.M. Denn, and R. Keunings

Center for Advanced Materials
Lawrence Berkeley Laboratory
and
Department of Chemical Engineering
University of California
Berkeley, California 94720

and

G.E. Molau and J. Ramos

The Dow Chemical Company
Walnut Creek, California 94598

ABSTRACT

Profile development in isothermal drawing of hollow tubes is studied using finite-element and asymptotic analyses. The transition from die flow to extensional flow of an annulus occurs over a distance comparable to the annular thickness. Considerable extrudate swell can occur with the flow rearrangement, and the final ratio of inner to outer radius can fall below that at the die despite an increase in this ratio over the entire draw zone. Asymptotic "thin-filament" equations describe the flow beyond the region of flow rearrangement.

INTRODUCTION

The extrusion and drawing of hollow tubes from molten polymers are similar to the processes of extrusion and drawing of textile fibers. As in fiber processing, there are three distinct regions that must be analyzed: the region of shear flow and profile rearrangement in and near the die or spinneret, the melt drawing region, and the region near the point of solidification. The major difference between the processing of hollow tubes and textile fibers is the additional degree of freedom afforded by the ability to impose an internal pressure in the hollow tube. This additional degree of freedom makes it possible, in principle, to control both the outer and inner radii of the drawn hollow tube.

The melt drawing region for textile fibers has been analyzed using an asymptotic analysis known as the thin filament equations. These equations are not valid in the region of flow rearrangement and extrudate swell near the spinneret, but finite-element methods have been used to study the flow in that region. The general conclusion is that the two methods give comparable results in the region of overlap, thus validating the use of the asymptotic analysis and establishing the appropriate initial state for the thin filament equations. These approaches to the simulation of fiber spinning are discussed in a recent chapter on computational methods (Denn, 1984), where complete references may be found. Little has been done regarding the solidification region, and most simulations take solidification to occur instantaneously, without any enthalpy change, at a specified temperature.

We describe here analyses of the rearrangement and melt drawing regions of hollow tubes. The approach is similar to that used for textile fibers except that the asymptotic analysis is modified by the presence of the in-

ternal pressure and the finite element treatment involves two free surfaces. One important conclusion with regard to processing is that the annular extrudate swell makes the rearrangement region more important in this process than in textile fiber spinning.

FORMULATION

The hollow tube is shown schematically in Fig. 1. For axisymmetric steady flow the equations for conservation of mass and momentum are as follows:

$$\frac{1}{r}\frac{\partial}{\partial r}(\rho r v_r) + \frac{\partial}{\partial z}(\rho v_z) = 0 \tag{1}$$

$$\rho\left(v_r \frac{\partial v_r}{\partial r} + v_z \frac{\partial v_r}{\partial z}\right) = -\frac{\partial p}{\partial r} + \frac{1}{r}(r\tau_{rr}) - \frac{\tau_{\theta\theta}}{r} + \frac{\partial \tau_{rz}}{\partial z} \tag{2a}$$

$$\rho\left(v_r \frac{\partial v_z}{\partial r} + v_z \frac{\partial v_z}{\partial z}\right) = -\frac{\partial p}{\partial z} + \frac{1}{r}\frac{\partial}{\partial r}(r\tau_{rz}) + \frac{\partial \tau_{zz}}{\partial z} + \rho g \tag{2b}$$

v_r and v_z are the r- and z-components, respectively, of the velocity vector $\underset{\sim}{v}$. The symbol g denotes the gravitational acceleration; the drawing direction is assumed to be vertical. τ_{ij} is the extra-stress, and p is the isotropic pressure; the total stress σ_{ij} is

$$\sigma_{ij} = -p\delta_{ij} + \tau_{ij} \tag{3}$$

where δ_{ij} equals unity when i and j are the same, and zero otherwise.

There are free-surface boundary conditions on both the velocity and the stress. The velocity condition is that there be no flow through the surface, or $\underset{\sim}{n}\cdot\underset{\sim}{v} = 0$ at $r = R_o$ and R_i (where R_i and R_o are the values of the inner and outer radius, respectively, at any point down the spinline); this is equivalent to

$$v_r = R_o' v_z \text{ at } r = R_o \tag{4a}$$

$$v_r = R_i' v_z \text{ at } r = R_i \tag{4b}$$

where R' denotes $\frac{dR}{dz}$. The stress conditions are most easily expressed in terms of the tangential and normal tractions, $\underset{\sim}{\sigma}_t$ and $\underset{\sim}{\sigma}_n$, respectively:

$$\underset{\sim}{\sigma}_n = \underset{\sim}{0}\ ,\ \underset{\sim}{\sigma}_t = -\rho_a |\underset{\sim}{v} - \underset{\sim}{v}_a| C_D \text{ at } r=R_o \tag{5a}$$

$$\underset{\sim}{\sigma}_n = -p_i\ ,\ \underset{\sim}{\sigma}_t = \underset{\sim}{0} \text{ at } r=R_i \tag{5b}$$

$\underset{\sim}{v}_a$ and ρ_a are the velocity and density of the ambient air. and C_D is an air-drag coefficient. p_i is the internal pressure (gauge).

The temperature field is assumed to be axisymmetric, axial conduction is neglected relative to convection, radial convection is neglected relative to conduction, and dissipation is assumed to be negligible. The energy equation is then

$$\rho v_z c_p \frac{\partial T}{\partial z} = k \frac{1}{r} \frac{\partial}{\partial r} \left(r \frac{\partial T}{\partial r} \right) \tag{6}$$

There is no heat transfer to the inner core, while heat transfer to ambient air at temperature T_a is described by a heat transfer coefficient, h. The boundary conditions are therefore

$$\frac{\partial T}{\partial r} = 0 \text{ at } r=R_i \tag{7a}$$

$$-k \frac{\partial T}{\partial r} = h(T-T_a) \text{ at } r=R_o \tag{7b}$$

THIN FILAMENT EQUATIONS

The thin filament equations are obtained by averaging Eqs. (1) and (2) over the cross-section at each value of z. The average $\bar{\psi}(z)$ of a variable

$\psi(r,z)$ is defined as

$$\bar{\psi}(z) = \frac{1}{\pi(R_o^2 - R_i^2)} \int_{R_i}^{R_o} 2\pi r \psi(r,z) dr \tag{8}$$

In computing derivatives with respect to z of averaged quantities, it is important to recall that both limits of integration are functions of the independent variable.

In averaging Eqs. (1) and (2) the following approximations are required. ($\bar{v}$ denotes $\bar{v}_z$.):

(i) $\frac{dR_o}{dz}, \frac{dR_i}{dz} \ll 1$

(ii) $\overline{v_z^2} \approx \bar{v}^2$

(iii) $\frac{d}{dz} \int_{R_i}^{R_o} 2\pi r^2 \tau_{rz} dr \approx 0$

(iv) inertial term can be neglected in the r-component of the averaged momentum equation.

Averaging of the continuity and z-momentum equations is straightforward. The r-component of momentum is averaged by multiplying each term by $2\pi r^2$ (rather than by $2\pi r$ because of the r^{-1} that appears in several terms) and integrating. Averaging of the convection term in Eq. (6) requires the assumption that v_z and the physical properties are independent of r. The resulting thin filament equations are then as follows:

$$w = \pi(R_o^2 - R_i^2)\rho\bar{v} = \text{constant} \tag{9}$$

$$w \frac{d\bar{v}}{dz} = \frac{d}{dz} \{\pi(R_o^2 - R_i^2)[\bar{\tau}_{zz} - \frac{1}{2}(\bar{\tau}_{rr} + \bar{\tau}_{\theta\theta})]\} - \pi R_o \rho_a \bar{v}^2 C_D + \pi(R_o^2 - R_i^2)\rho g \tag{10}$$

$$\frac{R_o R_i}{R_o^2 - R_i^2} p_i = \frac{1}{2}(\bar{\tau}_{\theta\theta} - \bar{\tau}_{rr}) \tag{11}$$

$$w c_p \frac{d\bar{T}}{dz} = -2\pi h R_o(\bar{T} - T_a) \tag{12}$$

$$\bar{\sigma}_{zz} = \frac{R_i^2}{R_o^2 - R_i^2} p_i + \bar{\tau}_{zz} - \frac{1}{2}(\bar{\tau}_{rr} + \bar{\tau}_{\theta\theta}) \tag{13}$$

Equations (9), (10), and (12) are identical to the thin filament equations for textile fibers, except for the replacement of R^2 by $R_o^2 - R_i^2$ to account for the hollow center. Equation (11) accounts for the hoop stress resulting from the internal pressure, and is required in order to provide an independent equation for the additional variable in the hollow tube process. It is to be noted that in general $\bar{\tau}_{\theta\theta} \neq \bar{\tau}_{rr}$.

INELASTIC LIQUIDS

A constitutive equation for the extra-stress is required in order to complete the description. Here the kinematical assumption $v_z = \bar{v}(z)$ must be made explicitly. The average stresses are then computed as follows for an inelastic liquid in which the only rheological parameter is a single non-Newtonian viscosity:

$$\bar{\tau}_{zz} - \frac{1}{2}(\bar{\tau}_{rr} + \bar{\tau}_{\theta\theta}) = 3\eta \frac{d\bar{v}}{dz} \tag{14}$$

$$\bar{\tau}_{\theta\theta} - \bar{\tau}_{rr} = - \frac{4\eta \ \ell n \ (R_i/R_o)}{R_o^2 - R_i^2} \frac{d}{dz} (R_i^2 \bar{v}) \tag{15}$$

ANALYTICAL RESULTS

Many of the analytical solutions to the thin filament equations for textile fiber spinning apply without change to the equations for drawn hollow tubes. For isothermal, low speed (no inertia or air drag) drawing of a Newtonian hollow tube without significant gravitational force, the velocity varies exponentially with distance:

$$\bar{v} = v_o \exp \left(\frac{Bz}{r_o - r_i}\right) \tag{16}$$

$$B = \frac{F - \pi r_i^2 p_i}{3\pi\eta v_o (r_o + r_i)} \tag{17}$$

Here r_i and r_o are the values of the inner and outer radius, respectively, at $z=0$, and v_o is the average velocity at $z=0$. F is the tensile force applied to draw the hollow tube. Clearly the relative importance of the internal pressure is governed by the dimensionless ratio $\pi r_i^2 p_i/F$; drawdown will be very slow as this group becomes of order unity, and the tube wall will thicken for values greater than unity. The asymptotic solutions for low speed, isothermal spinning of a Maxwell fluid (Denn et al., 1976) similarly apply, with a linear velocity profile and a maximum drawdown in the limit of large applied force.

One of the immediate consequences of Eqs. (9), (11), and (15) for $p_i > 0$ is

$$\frac{d}{dz} \left(\frac{R_i}{R_o}\right) > 0 \tag{18}$$

This is of particular processing significance, since control of R_o and R_i individually is important. It is found experimentally, in fact, that R_i/R_o at the takeup in a drawn thin hollow filament is about twenty percent less than the value at the die. We shall return to this point in the discussion of profile rearrangement near the die.

A further consequence of these equations is that, when $p_i = 0$, both $R_i^2 \bar{v}$ and $R_o^2 \bar{v}$ must remain constant. This result is useful as a check on the internal consistency of computational algorithms.

Finally, with standard correlations for the heat transfer coefficient, Eq. (12) for the temperature is insensitive to the kinematics, and the approximate solution given by Fisher and Denn (Denn, 1984) for the temperature profile and the point of solidification will apply directly for moderate drawdowns.

HOLLOW FIBER SPINNING

A typical simulation using the thin filament equations is illustrated in Figs. 2 and 3. The polymer properties were taken to be those of 0.67I.V. poly(ethylene terephthelate), with the temperature-equivalent Newtonian viscosity given by Gregory. Kase and Matsuo's heat transfer coefficient and Matsuo's correlation for air drag were used (Denn, 1984). The relevant operating parameters are given in Table 1. The general shapes of the velocity and temperature profiles are typical of those computed for the spinning of PET fibers. The very large area reduction ratios and relatively slow spinning speeds are typical of hollow fiber processing. The takeup speed is in the range where inertial and air drag effects are first expected to influence the profile development, and the force in fact varies by only about 10 percent over the length of the draw zone. The factor $\pi r_i^2 p_i/F$ (using the value of F at

Input Variables

Extrusion temperature	295°C
Solidification temperature	70°C
Ambient air temperature	30°C
Quench air velocity	0.2 m/s
Throughput	6.8 mm^3/s
Spinneret dimensions, r_o	1.0 mm
r_i	0.6 mm
Internal pressure, p_i	27 Pa
Takeup speed	14 m/s
Area reduction ratio	4140

Computed Variables

Spinneret stress	0.845 kPa
Takeup stress	3830 kPa
B	0.17
$\pi r_i^2 p_i / F$	0.018

Table 1
Variables for simulation of melt spinning of a poly(ethylene terephthalate) hollow fiber

z=0) is only equal to 0.018, so the internal pressure has little effect on the profile development and R_i/R_o increases only slightly over the length of the draw zone.

FINITE ELEMENT CALCULATIONS

Behavior in the region near the spinneret was analyzed by obtaining numerical solutions to Eqs. (1) and (2) using POLYFLOW$^{(R)}$, a finite element code developed at the Université Catholique de Louvain for the numerical simulation of viscoelastic flows (Crochet, 1982). The code is based on algorithms proposed in Crochet and Keunings (1980, 1982) and Keunings and Crochet (1984) and described in detail by Crochet et al. (1984). Although POLYFLOW$^{(R)}$ has nonisothermal capabilities, the solution was carried out only for isothermal flow and is therefore restricted to the region very close to the die where significant heat transfer will not yet have taken place. Because of the slow speeds in this region there is no need to include inertia or the air drag boundary condition.

Some typical calculations for a Newtonian fluid are shown in Figs. 4 through 6 for $r_i/r_o = 0.6$. The exponential velocity profile is achieved within one unit of distance, measured in units of the annular die thickness r_o-r_i, and the slope of the plot of $\ln \bar{v}$ versus $z/(r_o-r_i)$ is equal to B as defined in Eq. (16); thus, the validity of the thin filament equations for the draw zone is established. As in the case of textile fiber spinning (Keunings et al., 1983), the asymptotic solutions extrapolate approximately to the velocity corresponding to free extrudate swell (no imposed force), so this velocity could be used as the initial condition for the thin filament equations.

The effects governing the rearrangement region for the hollow fiber are illustrated in Fig. 5 with reference to the inner radius. R_i initially decreases because of extrudate swell. (Since R_o increases because of extrudate swell at the same time, $d(R_i/R_o)/dz$ must be negative in this region.) The positive internal pressure then causes R_i to increase. Finally, as the drawdown takes effect, R_i begins to decrease monotonically down the spinline. (It should be noted that the thin filament equations admit an initially increasing R_i, followed by a maximum, for a sufficiently large internal pressure.) The effect of internal pressure on the ratio R_i/R_o, as shown in Fig. 6, is substantially greater than the effect on the velocity and stress profile.

The conditions in Table 1 were simulated using POLYFLOW$^{(R)}$, taking the poly(ethylene terephthalate) to be Newtonian with all physical properties at the spinneret temperature. The results are shown in Figs. 7 and 8, together with the solution of the non-isothermal thin filament equations. The initial conditions for the thin filament equations were taken from the finite element solution at 0.3 mm, or 0.75 (r_o-r_i), from the die. The curves should deviate because the asymptotic analysis accounts for the changing physical properties with temperature. As would be expected, the initial slopes of the velocity profiles are the same, and the profiles are in close agreement over about 3 mm, or 7.5 (r_o-r_i). When the isothermal thin filament equations are used, however, velocity profiles are in close agreement over the entire spinline. The radius ratios deviate rapidly, and the thin filament solution over the axial distance shown is nearly the same for isothermal and nonisothermal cases. This rapid deviation may be explained by referring to Figures 4 and 6. For the case of zero internal pressure in Figure 6, the finite element solution approaches the thin filament prediction of $d(R_i/R_o)/dz = 0$ at about three

annular thicknesses from the die. However, Figure 4 shows that the finite element velocity profile matches the thin filament result ($\ell n\bar{v}$ linear in distance along the spinline) within about one annular thickness. This difference in the distance required for the thin filament and finite element results to agree quantitatively implies that the radius ratio profiles for the two methods should agree better if the starting point for the thin filament equations is moved farther down the spinline, and this is in fact observed.

Figure 8 illustrates what is perhaps the most important processing result from this study. The initial extrudate swell is the most important factor in determining the ultimate ratio R_i/R_o of a drawn hollow fiber. For the parameters used here this ratio is computed to be at or below the die ratio R_i/R_o, despite the fact that $d(R_i/R_o)/dz$ is positive over most of the length of the hollow fiber spinline. The stresses, however, and hence the structure, are developed in the draw zone.

The recoverable shear in the die for the conditions in Table 1 is 0.13, based on Gregory's relaxation time estimates for poly(ethylene terephthalate). This is a low level of viscoelasticity, and Keunings et al. (1983) saw only small effects at this level near the spinneret in textile fiber spinning; Gagon and Denn (1981) found that there were spinning conditions where the thin filament equations did show markedly different behavior between Newtonian and viscoelastic descriptions of poly(ethylene terephthalate) rheology. The conditions in Table 1 were simulated with POLYFLOW$^{(R)}$ using an Oldroyd B fluid model (Crochet and Keunings, 1982), with a viscosity ratio of 1/9 and a recoverable shear of 0.13. The computed velocity profiles for the Newtonian and Oldroyd B fluids were essentially the same. The difference was more apparent in the ratio R_i/R_o, however, as shown in Fig. 9, since this ratio is sensitive to small differences in extrudate swell. Figure 9 shows that the Oldroyd

fluid swells less than the Newtonian fluid. Crochet and Keunings (1980) have shown that, at this low level of viscoelasticity, Newtonian fluids exhibit slightly more die swell than viscoelastic fluids.

CONCLUSION

A complete analysis of the drawing of hollow tubes requires detailed consideration of the region of flow rearrangement near the die, as well as stress and area development in the draw region. The asymptotic thin filament equations for the latter predict average velocity and temperature profiles similar to those found previously for textile fibers. The evolution of the ratio of inner to outer radius in the draw region is governed by the extrudate swell, which will be sensitive to fluid rheology.

ACKNOWLEDGMENTS

The work done at Lawrence Berkeley Laboratory was supported in part by the Director, Office of Energy Research, Office of Basic Energy Sciences, Materials Sciences Division of the US Department of Energy under Contract No. DE-AC03-76SF00098. B.D. Freeman was a Berkeley Fellow and a National Science Foundation Fellow during the period of this work. M.M. Denn was a Visiting Professor at the University of Melbourne Chemical Engineering Department during the period of manuscript preparation. We are grateful to Prof. Marcel Crochet for making POLYFLOW$^{(R)}$ available to us, and to The Dow Chemical Company for permission to include their work.

REFERENCES

M.J. Crochet, "POLYFLOW, a Finite Element Program for the Simulation of Viscoelastic Flow: Theoretical Background" (1982) Unité de Mécanique Appliquée, Université Catholique de Louvain.

M.J. Crochet and R. Keunings, J. Non-Newtonian Fluid Mech. 7 (1980) 199.

M.J. Crochet and R. Keunings, J. Non-Newtonian Fluid Mech. 10 (1982) 339.

M.J. Crochet, A.R. Davies, and K. Walters, "Numerical Simulation of Non-Newtonian Flow," (1984), Elsevier, Amsterdam.

M.M. Denn, "Fiber Spinning," in J.R.A. Pearson and S. Richardson, eds., "Computational Analysis of Polymer Processing," (1983), Applied Sci. p.51, London.

M.M. Denn, C.J.S. Petrie, and P. Avenas, AIChE J. 21 (1975) 795.

D.K. Gagon and M.M. Denn, Polymer Eng. & Sci. 21 (1981) 844.

D.R. Gregory, Trans. Soc. Rheology 17 (1973) 191.

R. Keunings and M.J. Crochet, J. Non-Newtonian Fluid Mech. 14 (1984) 279.

R. Keunings, M.J. Crochet, and M.M. Denn, Ind. Eng. Chem. Fundamentals 22 (1983) 347.

CAPTIONS FOR FIGURES

Fig. 1 Schematic of a drawn hollow tube.

Fig. 2 Velocity profile from thin filament equations for conditions in Table 1.

Fig. 3 Temperature profile from thin filament equations for conditions in Table 1.

Fig. 4 Effect of internal pressure on velocity profile, finite element computation. $r_o = 1.0$, $r_i = 0.6$, $F = 2.0$, $v_o = 1.6$, $\eta = 1.0$.

Fig. 5 Effect of internal pressure on development of R_i for conditions in Fig. 4.

Fig. 6 Effect of internal pressure on the ratio R_i/R_o for conditions in Fig. 4.

Fig. 7 Velocity profile development for conditions in Table 1.

Fig. 8 Ratio R_i/R_o for conditions in Table 1.

Fig. 9 Effect of viscoelasticity on ratio R_i/R_o for conditions in Table 1.

FIGURE 1

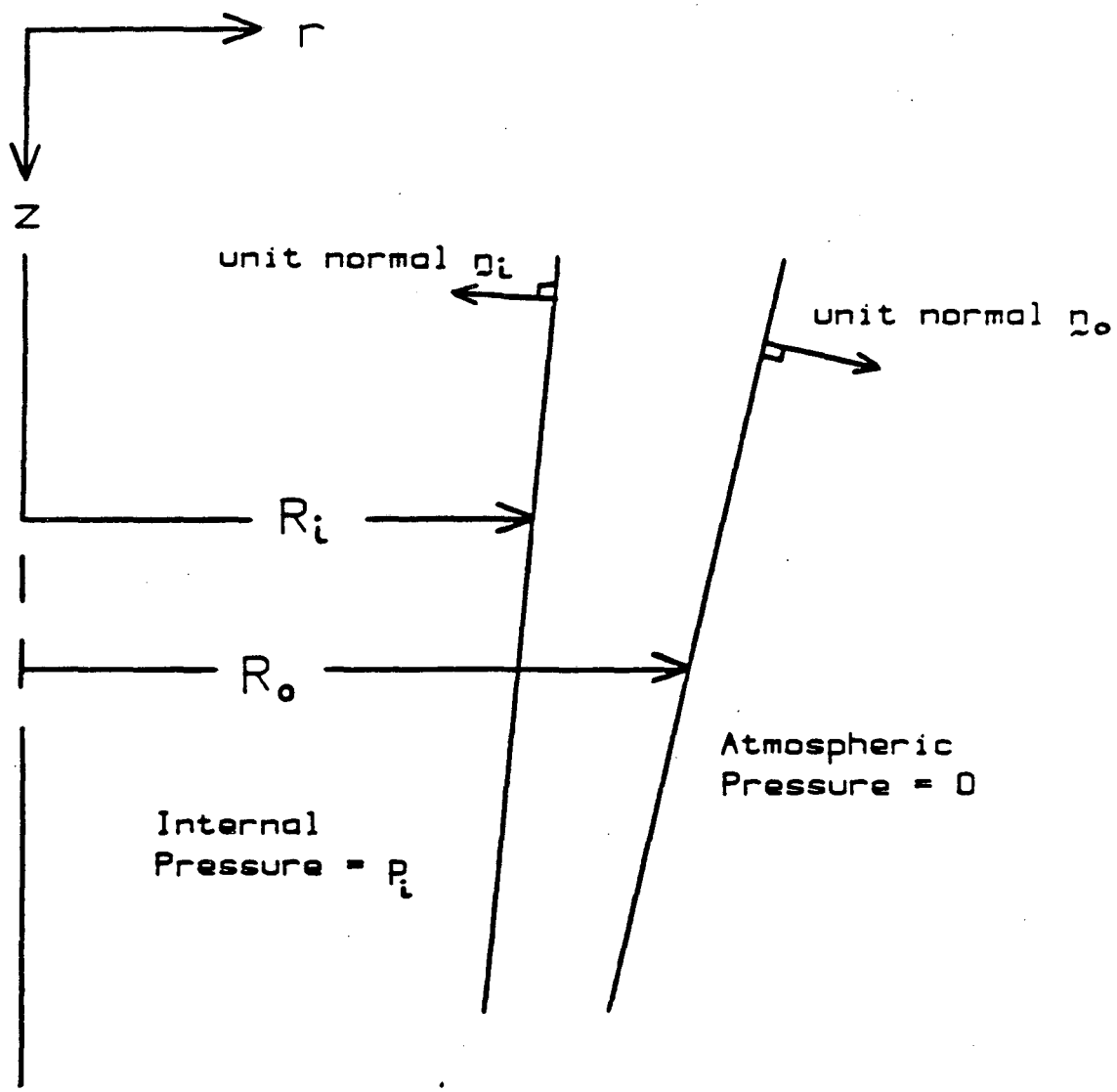
r
z
unit normal $\underset{\sim}{n}_i$
unit normal $\underset{\sim}{n}_o$
R_i
R_o
Atmospheric
Pressure = 0
Internal
Pressure = p_i

FIGURE 2

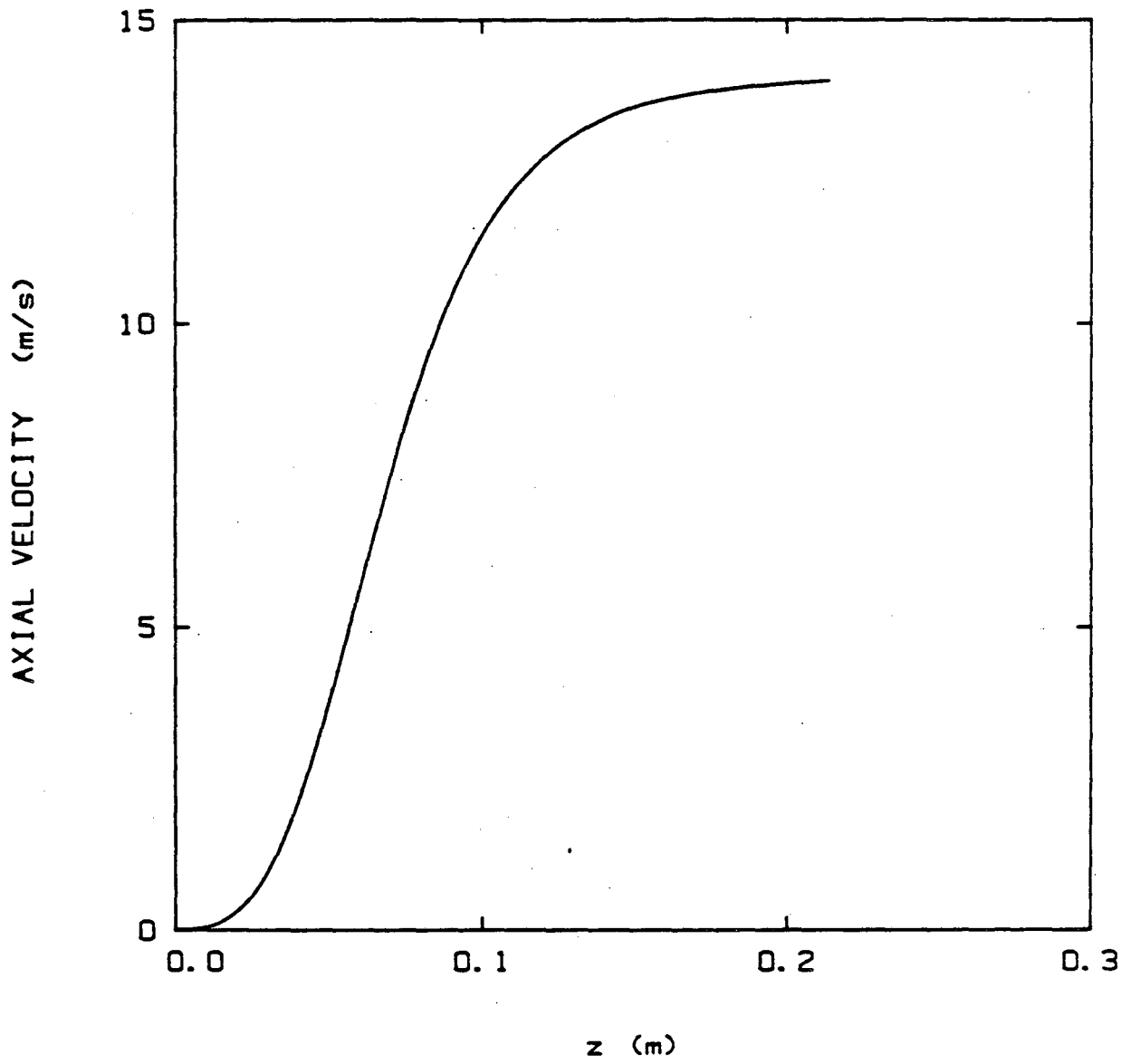

FIGURE 3

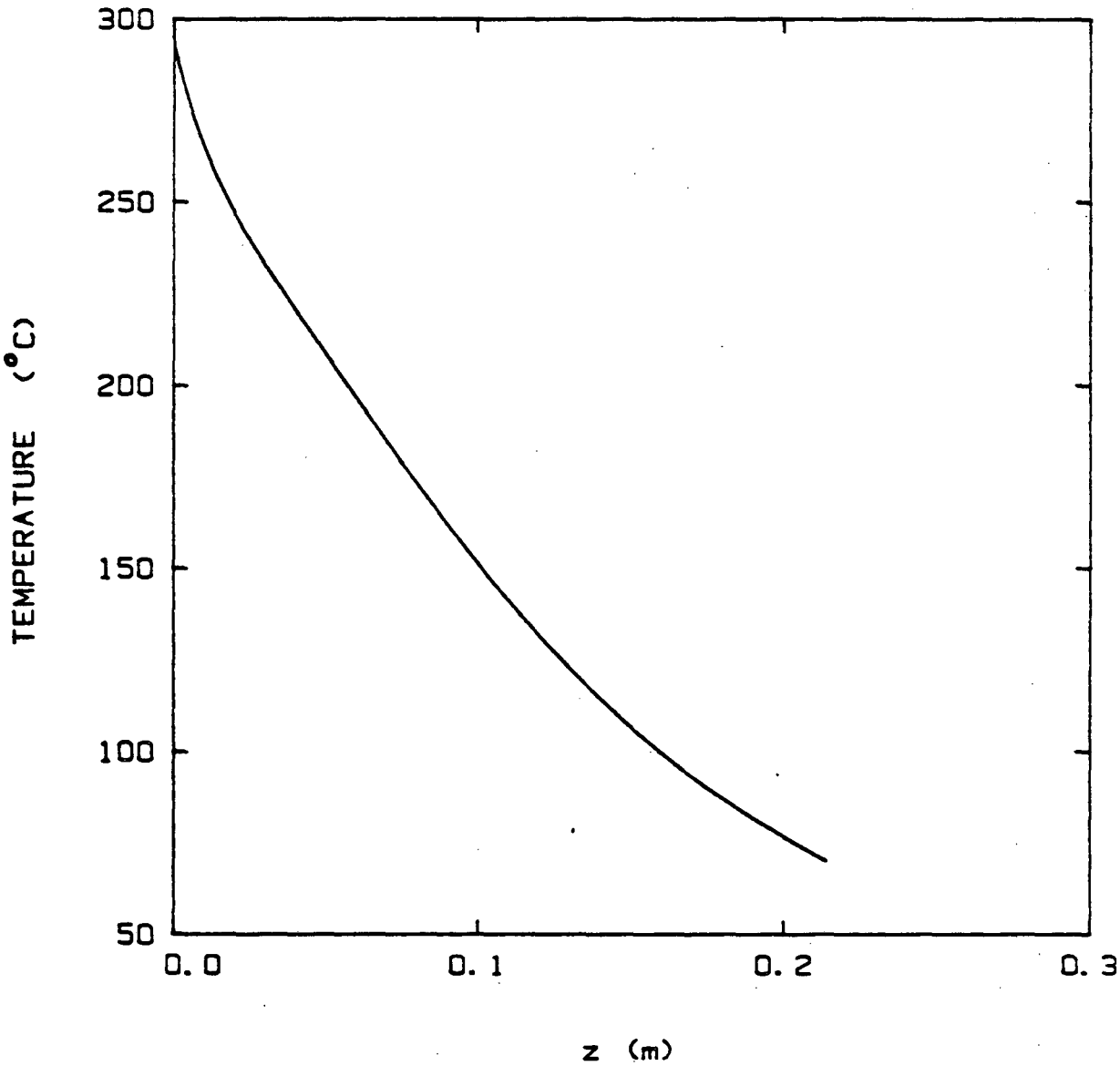

FIGURE 4

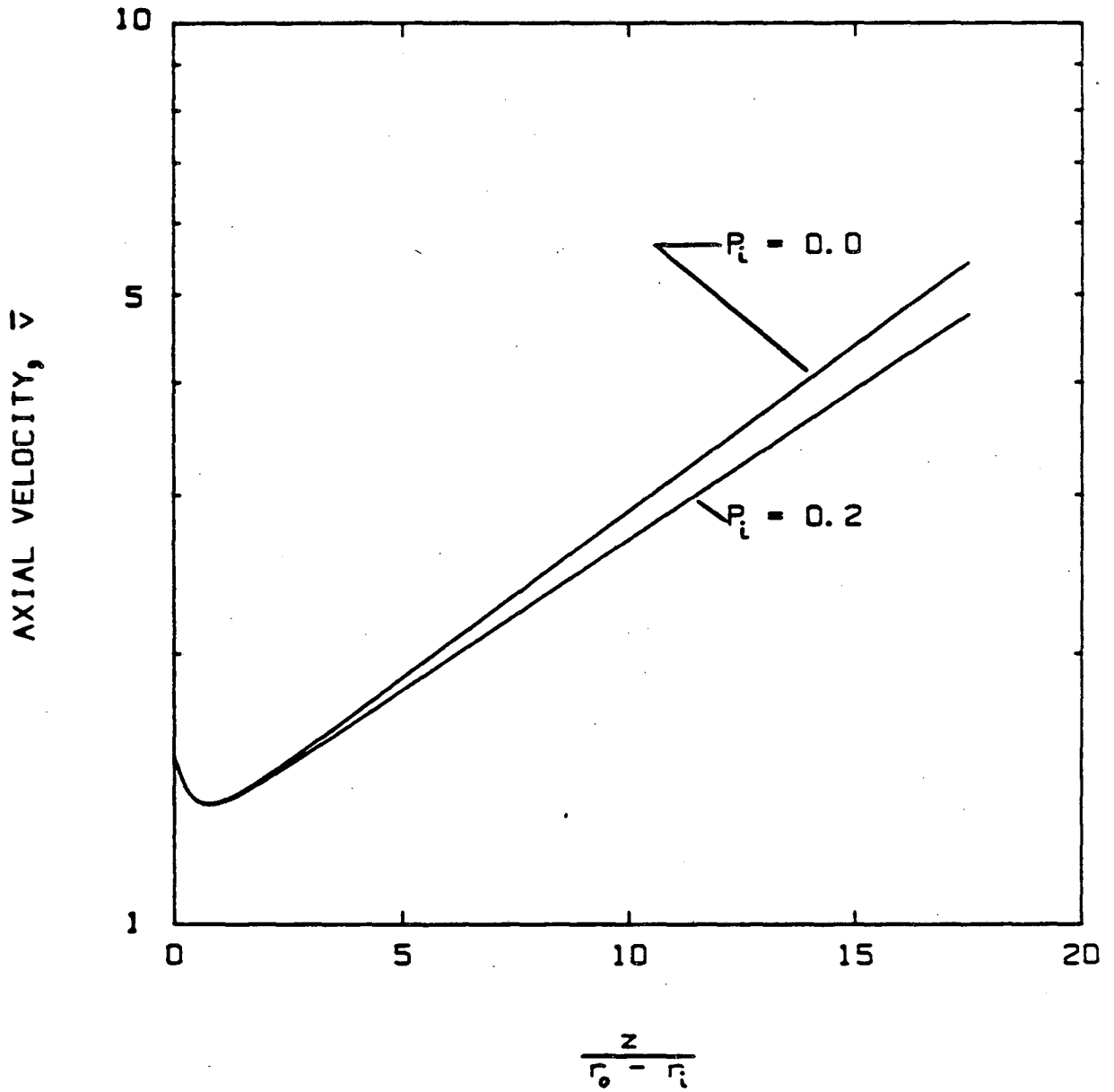

FIGURE 5

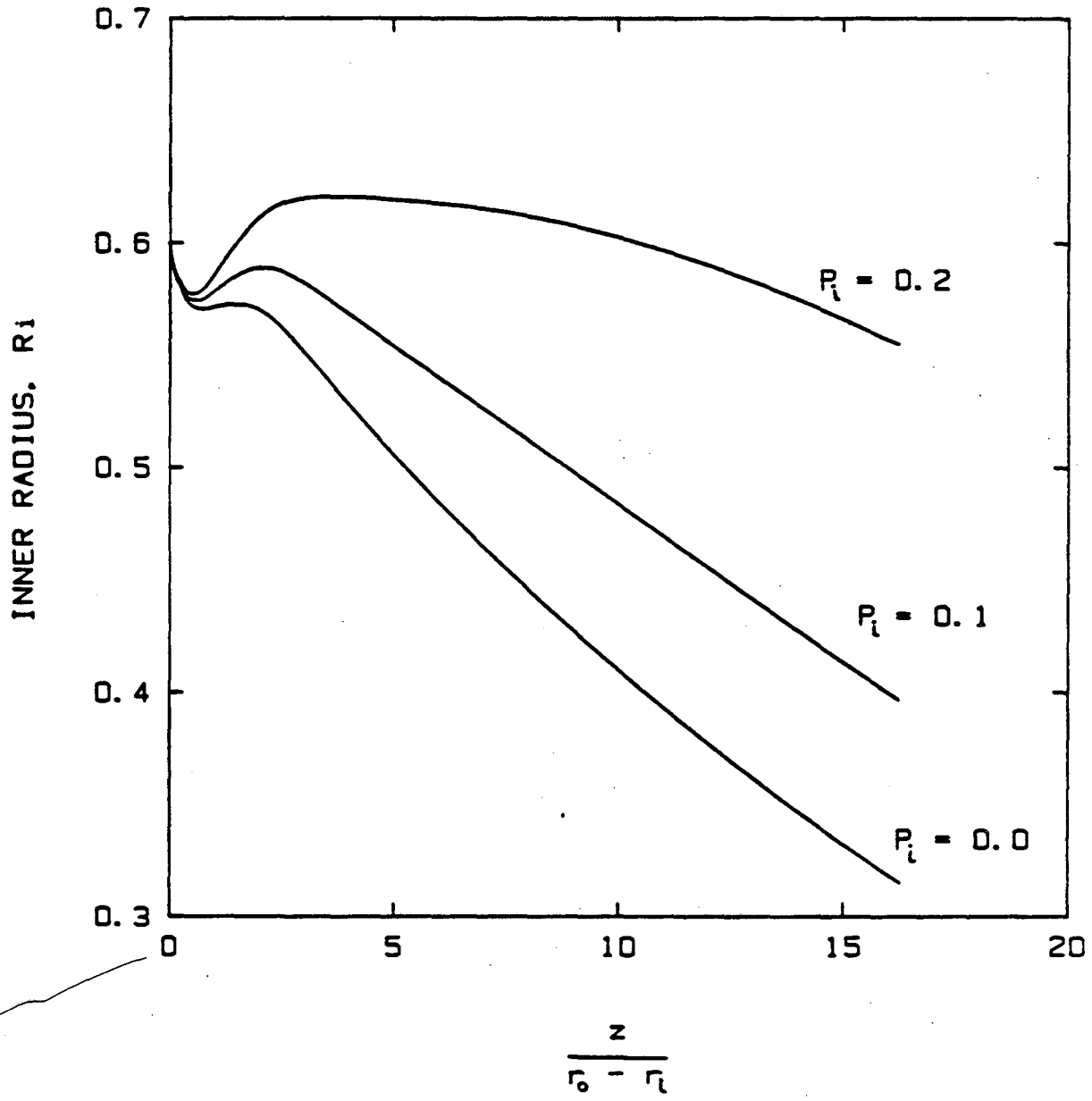
0.7
0.6
0.5
0.4
0.3
INNER RADIUS, Ri
P_i = 0.2
P_i = 0.1
P_i = 0.0
0
5
10
15
20
$\frac{z}{r_o - r_i}$

FIGURE 6

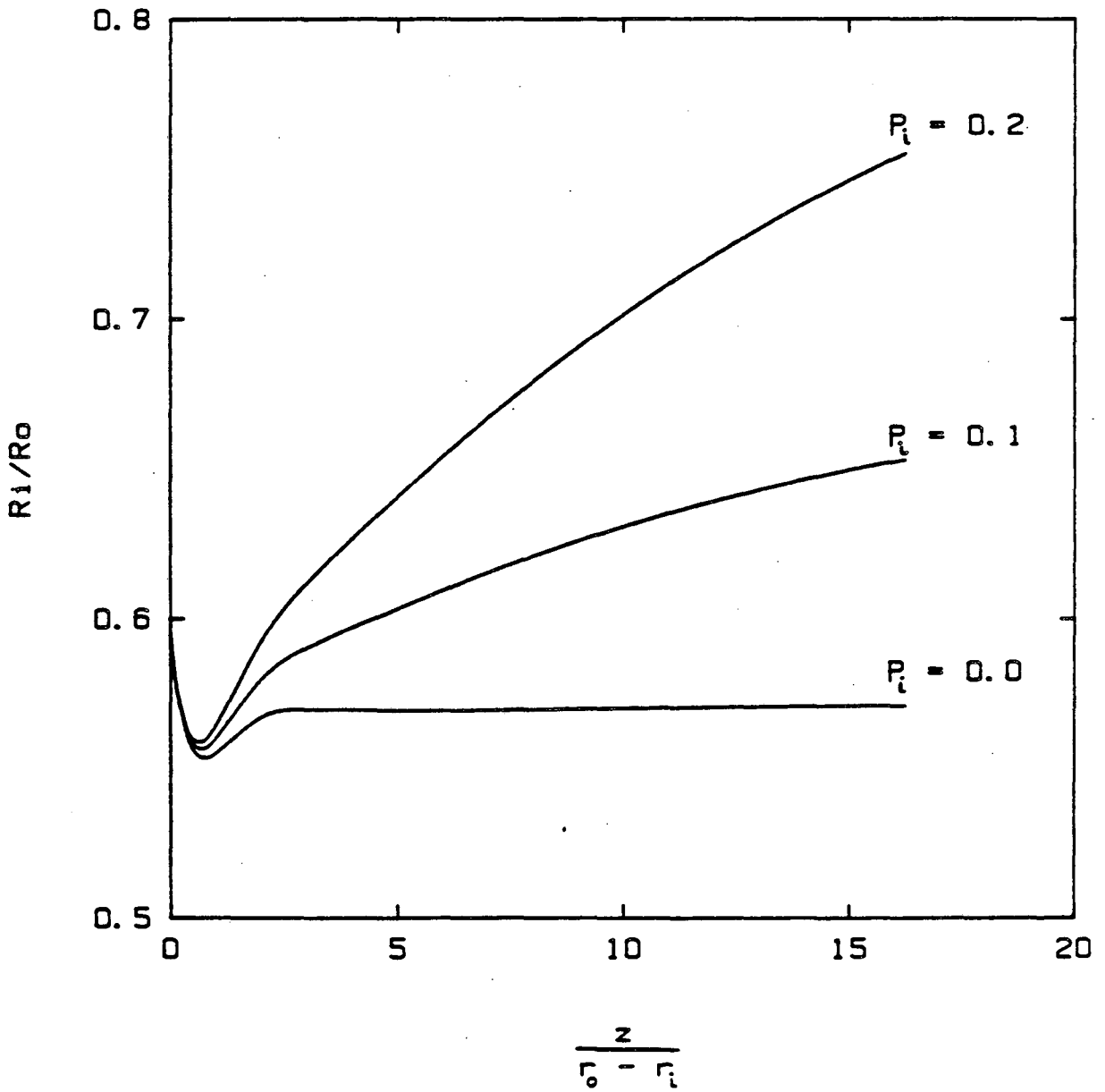

FIGURE 7

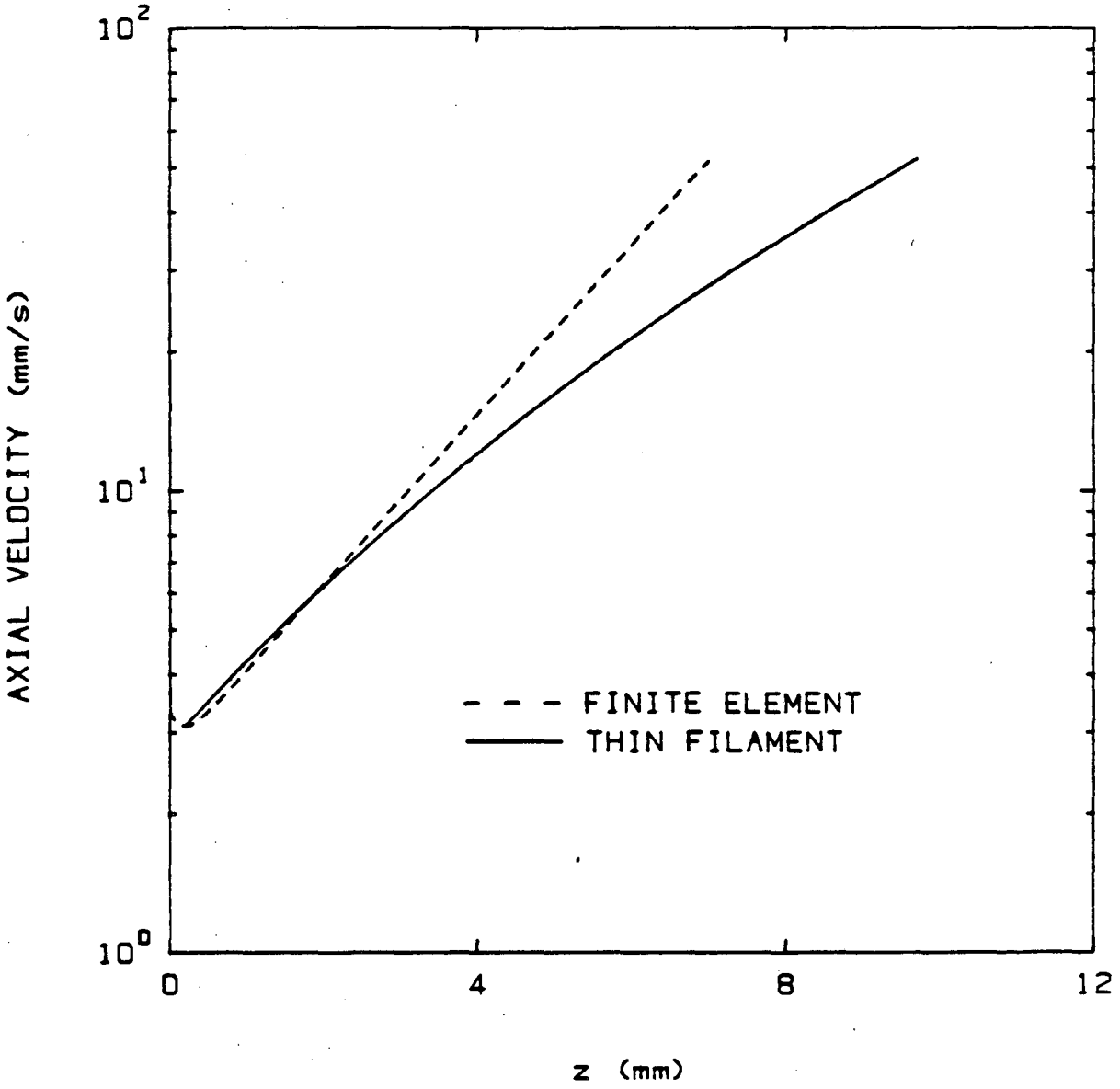
10^2
10^1
10^0
AXIAL VELOCITY (mm/s)
0
4
8
12
z (mm)
- - - FINITE ELEMENT
THIN FILAMENT

FIGURE 8

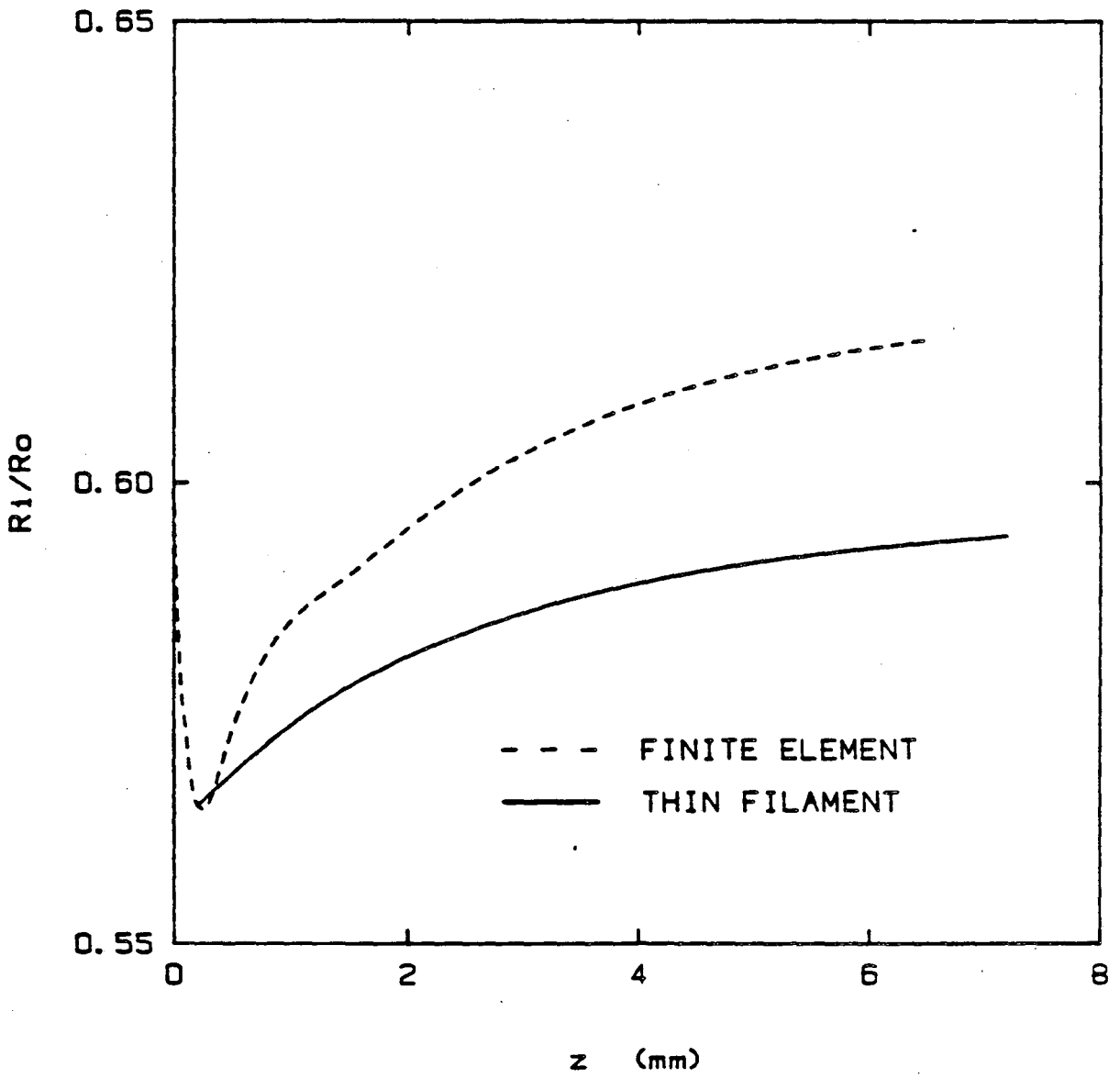

FIGURE 9

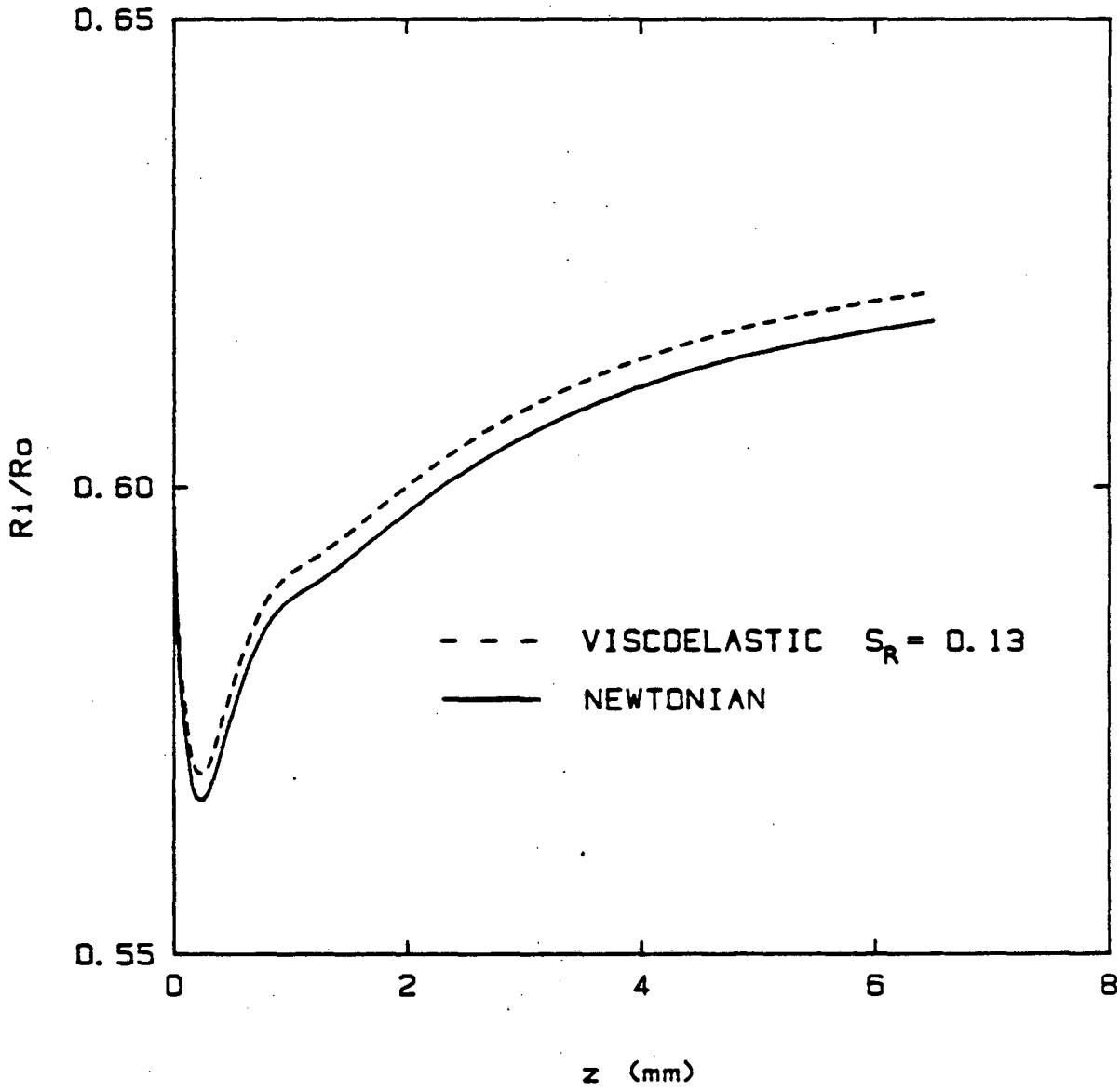

LAWRENCE BERKELEY LABORATORY
TECHNICAL INFORMATION DEPARTMENT
UNIVERSITY OF CALIFORNIA
BERKELEY, CALIFORNIA 94720